Optics Communications 392 (2017) 1–6

Contents lists available at ScienceDirect

Optics Communications

journal homepage: www.elsevier.com/locate/optcom

A portable confocal hyperspectral microscope without any scan or tube lens and its application in fluorescence and Raman spectral imaging

Jingwei Li[a,b], Fuhong Cai[a,b,c,*], Yongjiang Dong[a,b], Zhenfeng Zhu[a,b], Xianhe Sun[a,b], Hequn Zhang[a,b], Sailing He[a,b,**]

[a] Centre for Optical and Electromagnetic Research, State Key Laboratory for Modern Optical Instrumentation, Zhejiang University, Hangzhou 310058, China
[b] Joint Research Center of Photonics of the Royal Institute of Technology, Lund University and Zhejiang University (JORCEP), Hangzhou 310058, China
[c] Department of Electrical Engineering, College of Mechanical and Electrical Engineering, Hainan University, Hainan 570228, China

ARTICLE INFO

Keywords:
Portable
Detection efficiency
Hyperspectral imaging
Raman spectral imaging

ABSTRACT

In this study, a portable confocal hyperspectral microscope is developed. In traditional confocal laser scanning microscopes, scan lens and tube lens are utilized to achieve a conjugate relationship between the galvanometer and the back focal plane of the objective, in order to achieve a better resolution. However, these lenses make it difficult to scale down the volume of the system. In our portable confocal hyperspectral microscope (PCHM), the objective is placed directly next to the galvomirror. Thus, scan lens and tube lens are not included in our system and the size of this system is greatly reduced. Furthermore, the resolution is also acceptable in many biomedical and food-safety applications. Through reducing the optical length of the system, the signal detection efficiency is enhanced. This is conducive to realizing both the fluorescence and Raman hyperspectral imaging. With a multimode fiber as a pinhole, an improved image contrast is also achieved. Fluorescent spectral images for HeLa cells/fingers and Raman spectral images of kumquat pericarp are present. The spectral resolution and spatial resolutions are about 0.4 nm and 2.19 μm, respectively. These results demonstrate that this portable hyperspectral microscope can be used in in-vivo fluorescence imaging and in situ Raman spectral imaging.

1. Introduction

Fluorescence/Raman imaging is one of the most important imaging technologies in biological imaging. Fluorescent signal can help to provide a high contrast image in biological study. Owing to its fingerprint characteristic to molecule structure, Raman imaging has been well-established as a useful tool in biology [1–3], pharmacology [4–8], and food-safety investigations [9,10]. Furthermore, fluorescence/Raman spectral imaging technology provide a 4D information (spatial and spectral) of a target, which has a great significance in pharmacology and biomolecular study [11]. Recently, by using imaging spectrometer and scanning method, hyperspectral imaging technology, with sub-nanometer spectral resolution and micrometer spatial resolution, has been developed [12–14]. Meanwhile, various portable fiber Raman probes has been used in biomedical applications, such as endoscopes and colonoscopies. Schwab and McCreery developed a fiber probe, consisting of a multitude of collections fibers surrounding a single excitation fiber, to improved collection efficiency [15]. And this arrangement is prevalently used and improved for Raman spectroscopy [16–21]. Dual fiber probe with optical filters was also investigated in order to prevent the reentry of specularly reflected laser light into collection fiber [22–24].

On the other hand, capable of optical sectioning and able to provide greater resolution than conventional imaging, confocal laser scanning microscope (CLSM) have been intensively investigated and applied in biological and medical imaging area. In a traditional CLSM, a rotated grating is utilized to perform spectral imaging. However, the spectral resolution is relatively low.

Since high spatial resolution hyperspectral imaging and fiber Raman probe have immense applications in biomedical and food-safety area, a portable confocal hyperspectral microscope (PCHM) is developed in this study. The system is aimed at utilizing the fiber spectrometer to achieve spectral image with a considerable collection efficiency. As fiber spectrometer usually has a low optical sensitivity compared with a high-end spectrometer which was widely used in previous investigations, it is necessary to improve the detection efficiency. In our PCHM, the galvomirror is placed directly next to the objective, though adopting the confocal detection mode. In this

* Corresponding author at: Department of Electrical Engineering, College of Mechanical and Electrical Engineering, Hainan University, Hainan 570228, China.
** Correspondence to: Joint Research Center of Photonics of the Royal Institute of Technology, Lund University and Zhejiang University, Hangzhou, China.
E-mail addresses: caifuhong@zju.edu.cn (F. Cai), sailing@zju.edu.cn (S. He).

http://dx.doi.org/10.1016/j.optcom.2017.01.031
Received 13 October 2016; Received in revised form 16 January 2017; Accepted 21 January 2017

way, the detection efficiency for signal light can be enhanced compared with the traditional confocal microscope setup with scan lens and tube lens. Meanwhile, the removal of the scan lens and tube lens further reduce the size of the system. We experimentally demonstrate the diverse hyperspectral image capability of this system by obtaining the fluorescence spectral image of cells and Raman spectral image of kumquat pericarp.

2. Methods and materials

2.1. Optical configuration of the portable confocal hyperspectral microscope

In a traditional CLSM, scan lens and tube lens are usually utilized to build up a conjugate relationship between the galvanometer and the back focal plane of the objective, to implement imaging with higher resolution and intensity homogeneity at the imaging sample. However, the employment of both scan lens and tube lens makes it difficult to scale down the system. Besides, scan lens and tube lens are used to expand the excited laser beam, but it would also scale down the diameter of signal light beam. Signal light beam will have a lager focal spot after passing though the focal lens before pinhole, thus would be partially blocked by the pinhole. Therefore, the existence of scan lens and tube lens reduce the detection efficiency. In addition, absorption and reflection of lens also deteriorate the detection of signal light. To improve the signal light detection efficiency and reduce the volume of this system, a PCHM is developed without using scan and tube lens.

The imaging system consists of a fiber-coupled laser source, an optical scanning units, a set of filters, an imaging objective and a detection module. Fig. 1(a) provides a schematic of the optical setup of the PCHM. Fig. 1(b) shows the corresponding photograph of the PCHM. A single-mode fiber-coupled 532 nm laser is collimated and injected into the system. Then it is deflected by a mirror mounted on a right-angle kinematic mirror mount (KCB1/M; THORLABS), and transmitted into a galvanometer mirror (GM) by a dichroic beam splitter (LPD02-532RU-25; Semrock), which is mounted on a kinematic dichroic filter mount (DFM/M; THORLABS). The galvanometric mirror is used to perform scanning imaging. The signal light emitted from the sample is collected by the same objective, and transmitted through the GM and dichroic beam splitter. A long pass edge filter (BLP01-532R-25; Semrock), which is assembled in DFM/M, is used to eliminate the excitation light source. Then the signal light is reflected by a mirror mounted on KCB1/M and focused into a multimode optical fiber by an aspheric achromatic lens (49–622; Edmund), which is mounted on a z-axis translation mount (SM1Z; THORLABS). Here, the fiber is utilized as a pinhole to reject the noise out of focus and is fixed on an SMA fiber adapter plate (SM1SMA; THORLABS), which is assembled on a thread cage plates (CP02/M, THORLABS). Finally, the signal is collected through the fiber by a detection module, which can be a photodiode (PD), a photomultiplier tube (PMT), or a spectrometer. The image processes are controlled by a home-made LABVIEW software running on a personal computer equipped with multifunctional data acquisition cards (NI USB-6356; National Instruments). As the GM raster scans the sample, the signal from each pixel is collected simultaneously and displayed on the computer screen in real time. Imaging can be performed in reflectance mode, fluorescence mode and Raman mode. A beam splitter is assembled in DFM/M when working in a reflectance mode, instead of a dichroic beam splitter when working in fluorescence mode or Raman mode. Commercially-available fiber spectrometer, USB2000+ and QE65000 (Ocean Optics) are utilized in this system in spectral mode, the spectral resolution of which are 1 nm and 0.4 nm, respectively.

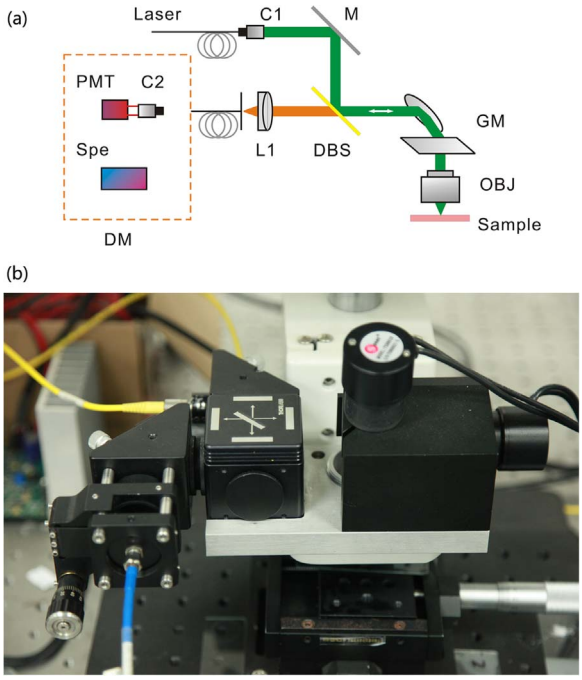

Fig. 1. (a) Schematic of the portable confocal spectral microscope. M: mirror. DBS: dichroic beam splitter. GM: galvanometer mirror. OBJ: objective. C1 and C2: fiber collimator. DM: detection module. L1: aspheric achromatic lens. (b) Photograph of the portable confocal spectral microscope tabletop implementation.

2.2. Materials

Polymer microspheres, red fluorescing, 1% solids, and Rhodamine 6G were purchased from Duke Scientific Corp and Sigma-Aldrich, respectively. HeLa cells were labeled with labeled with 2,3-Bis(4-(phenyl(4-(1,2,2-triphenylvinyl)phenyl)amino)phenyl) fumaronitrile(TTF)encapsulated organically modified silica (ORMOSIL) [25]. They were cultivated in Dulbecco minimum essential media (DMEM) with 10% fetal bovine serum (FBS), 1% penicillin, and 1% amphotericin B, at 37 °C and 5%, and were grown overnight on 35 mm petri dishes with cover slips. After 24 h, the diluted solution of about 25 μg/mL TTF-ORMOSIL nanoparticles was utilized to treat the HeLa cells for 30 min. Then the HeLa cells were washed thrice by phosphate buffered saline (PBS, pH=7.4, 10 mM) and treated with paraformaldehyde in for 15 min. After that, the cells were washed thrice by PBS again and the cover slips with cells were sealed with glycerin onto the glass slides.

3. Results and discussion

3.1. Characterization of lateral spatial resolution

The lateral spatial resolution of PCHM was characterized in reflectance mode by imaging a US Air Force (USAF) target (R1DS1P; THORLABS). The sample was captured by a 20×1.0 NA (Numerical Aperture) water objective (N20X-PFH; Olympus), with entrance pupil about 20 mm. The diameter of the laser beam was adjusted to be 5 mm in this work, in order to make sure the whole excitation laser beam is able to transmit through the objective and focus on the sample during the laser scanning process. However, this results in a relatively lower resolution according to Rayleigh formula. Fig. 2(a) shows that the microscope can distinguish the group 7, element 6 of R1DS1P, in which the line width is 2.19 μm. As this is the minimum spacing of the test target, we believe the actual lateral resolution of this system is superior to 2.19 μm. According to the NA of objective and input laser, the theoretical spatial resolution is 1.3 μm (0.61×λ/NA×4), where the factor 4 stands for the ratio between entrance pupil and laser beam. Fig. 2(b) was obtained by using photodiode detector (PDA100A-EC; THORLABS) as the detection module, while Fig. 2(c) was obtained by

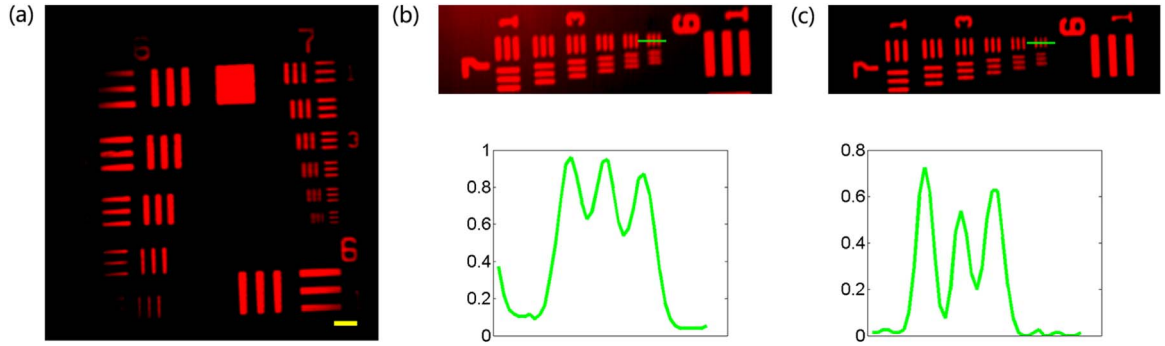

Fig. 2. (a) Reflectance image of a 1951 USAF resolution test target. Resolvable lines in element 6 of group 7 (2.19 μm). FOV is about 600×600 μm. Scan bar: 20 μm. (b) Reflective image of test bar detected directly by photo-diode detector (PD). (c) Reflective image of test bar detected by the same PD through a fiber with the diameter of 600 μm, which acts as a pinhole.

using confocal detection module. A fiber which has a core diameter of 600 μm is the pinhole and the same photodiode detector is served as the detection. Evidently, the latter has a better signal to background ratio. In summary, the lateral resolution of this system is superior to 2.19 μm, and with fiber as a pinhole, the image contrast of this system is greatly enhanced. The lateral resolution of 2.19 μm is adequate to be used in diagnosis of various skin and diseases [26,27] and biopsy [28].

3.2. Investigation of signal detection efficiency

Although having a relatively lower lateral resolution due to the smaller laser beam, the PCHM is believed to own an advantage of higher signal detection efficiency for its compact optical length. To verify this, we investigated the relationship between the fluorescence detection efficiency and the optical path in fluorescence mode. Herein, the aspheric achromatic lens and fiber were served as the confocal module. By changing the distance between the confocal module and dichroic beam splitter from 188 mm to 8 mm with a 30-millimeters interval, we detected a series of fluorescence intensity data for the polymer microspheres, which emits red fluorescence as mentioned in Section 2.B. Illuminated by a 532 nm laser, the fluorescence emission of the sample was detected with a photodiode detector. The core diameter of the fiber was 600 μm. At each detection, fluorescence intensity was measured ten times and then averaged to record the fluorescence intensity. Fig. 3(a) shows the relationship between the detection fluorescence and the optical path, namely the distance between the confocal module and dichroic beam splitter. It is obvious that the logarithm of detection fluorescence intensity increases as the length of optical path decreases, which indicates that reducing optical path is helpful to enhance fluorescence detection efficiency.

To further study the light detection efficiency of this system, we compared it with a traditional confocal microscope quantitatively. For comparison, a scan lens (LSM03-VIS, Thorlabs) and a tube lens (a doublet lens with the foci of 150 mm) were added into the system to act as a traditional system. 10 nM/L Rhodamine 6G solution was prepared as the sample. For both structure, the solution was illuminated by 532 nm laser through a 10×0.3 NA (UPlanFLN; Olympus) objective. And the focal power is 7.7 mW. The spectrum was obtained by utilizing the USB2000+ fiber spectrometer, with 500 ms integration time. Each spectrum was measured 5 times and then averaged. Spectra are presented in Fig. 3(b)–(d). The ratio between the detected intensity without and with 'scan and tube lens' is defined as enhancement factor here. As 600 μm fiber is utilized in the experiment, the enhancement factor is 2.95. In this case, the optical section is deteriorated and the system can detect the out of focus light. Thus a large part of the improvement is due to detection of out of focus light. When the fiber core diameter is 100 μm, the ability of optical section is improved, less out of focus light can be detected. Hence the enhancement factor is reduced to about 1.41. For the fiber with 62.5 μm core diameter, which is an acceptable pinhole size for traditional confocal microscope, the detection intensity is enhanced by about 25%. With 62.5 μm fiber, the system without scan and tube lens can be considered with confocal ability. As discussed before, this enhancement is partly attributed to the absent of lens' absorption and reflection. Besides, scan lens and tube lens would scale down the diameter of signal light beam, make its focal spot larger. Based on the above discussion, as the using of 62.5 μm fiber, our system can be considered with confocal ability but with less detection efficiency. In this paper, in order to measure the fluorescence/Raman spectral imaging from the surface of bio-sample, 600 μm fiber is applied in the system to improve the detection rate.

3.3. Fluorescence intensity and spectral imaging

In this section, the PCHM was used for fluorescence imaging. The fluorescence spectrum of the HeLa cells labeled with TTF-ORMOSIL is shown in Fig. 4(a). The laser power for fluorescence imaging of HeLa cells labeled by TTF-ORMOSIL at the foci was about 0.15 mW. The fluorescence emission of HeLa cells was detected with a PMT (H10721-01; Hamamatsu Photonics). Signals were pre-amplified before digitization (C7319; Hamamatsu Photonics). Fig. 4(b) shows the fluorescence image of HeLa cells, from which we can see the morphology of HeLa cells clearly, indicating that the system is capable of achieving cellular resolution. The dwell time of each pixel was 20us, and image size was 256×256 pixels. The spectral image of the cell was also investigated to demonstrate the spectral imaging capability of the system. The system was also performed in spectral mode. 532 nm laser was utilized to excite the fluorescence of cells through the 20× water objective. Fluorescence emission from cells was detected by a spectrometer (USB2000+; Ocean Optics) instead of the PMT, through the fiber with a core diameter of 600 μm. The spectral resolution of the spectrometer was 1 nm, and the spatial lateral resolution was 2.19 μm, as mentioned in Section 3.A. The dwell time of each pixel, namely, the integration time of each pixel was 100 ms. Image size was 128×256 pixels. Figure (c) shows the fluorescence spectral image of Hela cells at 651.3 nm, in which the cell with higher TTF-ORMOSIL concentration has a deeper red color. This image can be well identified, indicating the spectral resolution of hyperspectral image is equal to the spectral resolution of spectrometer. Fig. 4(d) shows spectral image of Hela cells integrated from 625 nm to 675 nm. Obviously, Fig. 4(d) has better signal to noise ratio, compared with Fig. 4(c). The experiment results demonstrate the PCHM can be used to obtain fluorescence spectral images of cancer cells, which has the potential to be applied in pathology.

3.4. In-vivo fluorescence intensity imaging

Furthermore, in order to demonstrate the in vivo imaging capability of this system, a fingerprint fluorescent intensity image was obtained. Herein, the index finger of a volunteer was illuminated by a 532 nm laser with the power of about 7 mW at the focal plane. Fig. 5(a) shows the fluorescence spectrum of the finger. Fig. 5(b) shows the fluores-

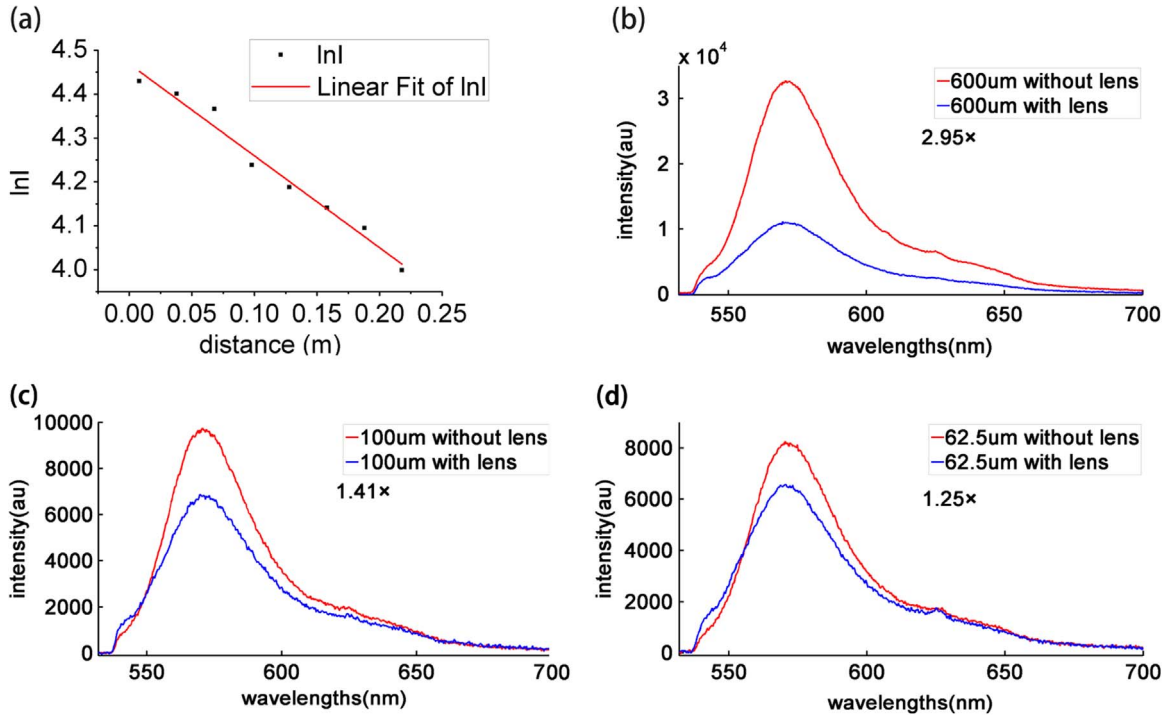

Fig. 3. (a) The relationship between the detection fluorescence and the optical length. LnI denotes the logarithm of detection fluorescence intensity. (b)–(d) represent fluorescence spectra of 10 nM/L Rhodamine 6 G by using fibers with 600 μm, 100 μm and 62.5 μm core diameter, the red curves represent the spectra without scan and tube lens, the blue curves represent the spectra with scan and tube lens.

cence image of index finger surface. The outline of the fingerprint is obvious, which indicates this portable system can be exploited to implement the in vivo fluorescent imaging of tissue objects. Furthermore, this system may be used in crime investigation, as constituents of the fingerprint residue itself (e.g., riboflavin) can result in fluorescence emission when illuminated by appropriate light sources [29]. In addition, by using confocal detection mode, the optical section effect helps to improve the image contrast. It is need to mention that, informed consent was obtained from the volunteer, and approval for the study protocol was granted by Center for Optical and Electromagnetic Research of Zhejiang University.

3.5. Raman spectral imaging

As mentioned above, a fiber spectrometer is used as the detection module in spectral mode. Hence, we can easily replace the detection for different purposes without finely adjusting the system. In the last section, a fiber Raman spectrometer QE65000 with spectral range 479–660 nm is used as the detection module. Also, due to the high light detection efficiency, it is advantageous for this system to perform Raman spectral imaging.

A fresh kumquat was used as the sample, which is illuminated by a 532 nm laser through the 10×0.3 NA (UPlanFLN; Olympus) objective, as Fig. 6(a) depicts. Raman signal was detected by QE65000, after transmitting through the dichroic beam splitter. Excitation light was suppressed by the long pass edge filter. The spectral resolution of spectrometer was about 0.4 nm. And the integration time was set to 1 s. The spatial resolution was about 5.5 μm. Fig. 6(b) displays the Raman spectral image of a fresh kumquat with clean pericarps, featuring two bands at about 1152 cm^{-1} and 1522 cm^{-1}, attributed to carotenoid molecules contained in citrus fruits [30]. The Raman spectrum was obtained at a single point of clean pericarps, with the integral time of 1 s. This spectrum is the original spectrum of fresh kumquat after baseline correction without smoothing process. Fig. 6(c) shows the reflective intensity image of the kumquat pericarps, and the black region stands for the scar material on the pericarps. Dwell time of each pixel was 20 μs, and image size was 128×128 pixels, which is the same with Fig. 6(d). Fig. 6(d) shows the Raman spectral image of kumquat pericarps almost at the same region as in Fig. 6(c). In the red dotted rectangular region of Fig. 6(c), we can see that the distribution of light intensity is relatively uniform along the purple line, as the inset shows. However, in Fig. 6(d), there is an apparent fluctuation of Raman signal

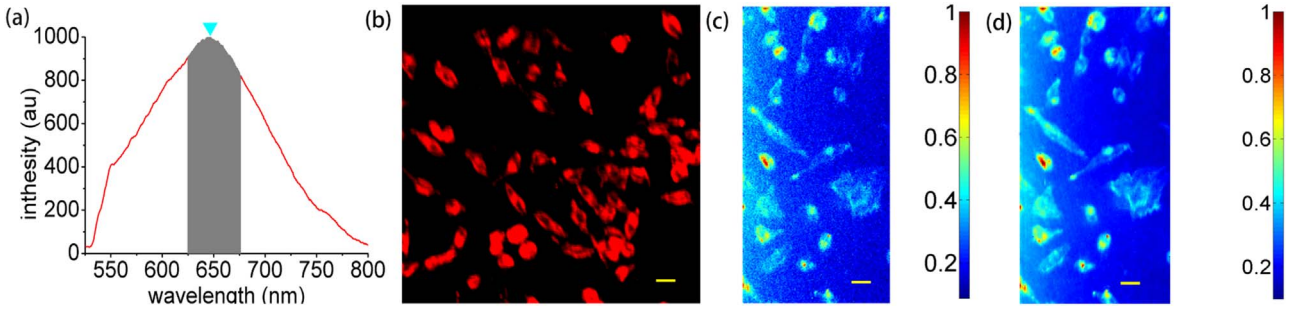

Fig. 4. (a) Fluorescence spectrum of HeLa cells labeled by TTF-ORMOSIL. (b) Fluorescence image of HeLa cells labeled by TTF-ORMOSIL. Pixel dwell time: 20us. Image size: 256×256 pixels. Scan bar: 20 μm. (c) Fluorescence spectral image of HeLa cells at the wavelength of 651.3 nm, indicating by the triangle in (a). Image size: 128×256 pixels. (d) Fluorescence spectral image of HeLa cells integrated from 625 nm to 675 nm, as shown in (a). Image size: 128×256 pixels.

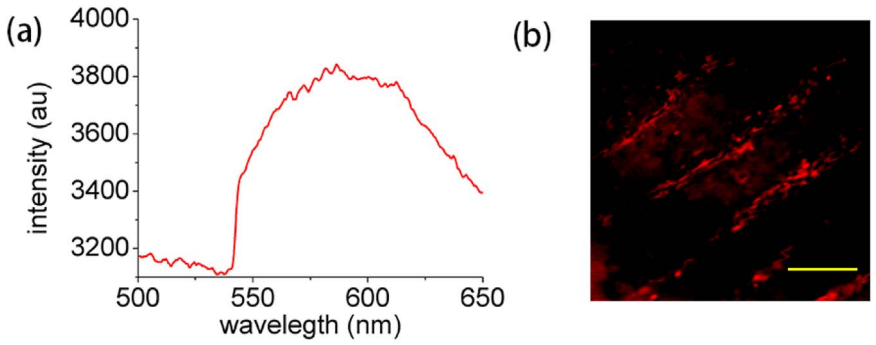

Fig. 5. (a) Fluorescence spectrum of index finger. The excitation laser power is about 7 mW, while the integration time is 0.5 s (b) Fluorescence image of index finger surface, by the utilization of confocal setup. Scan bar : 500 μm.

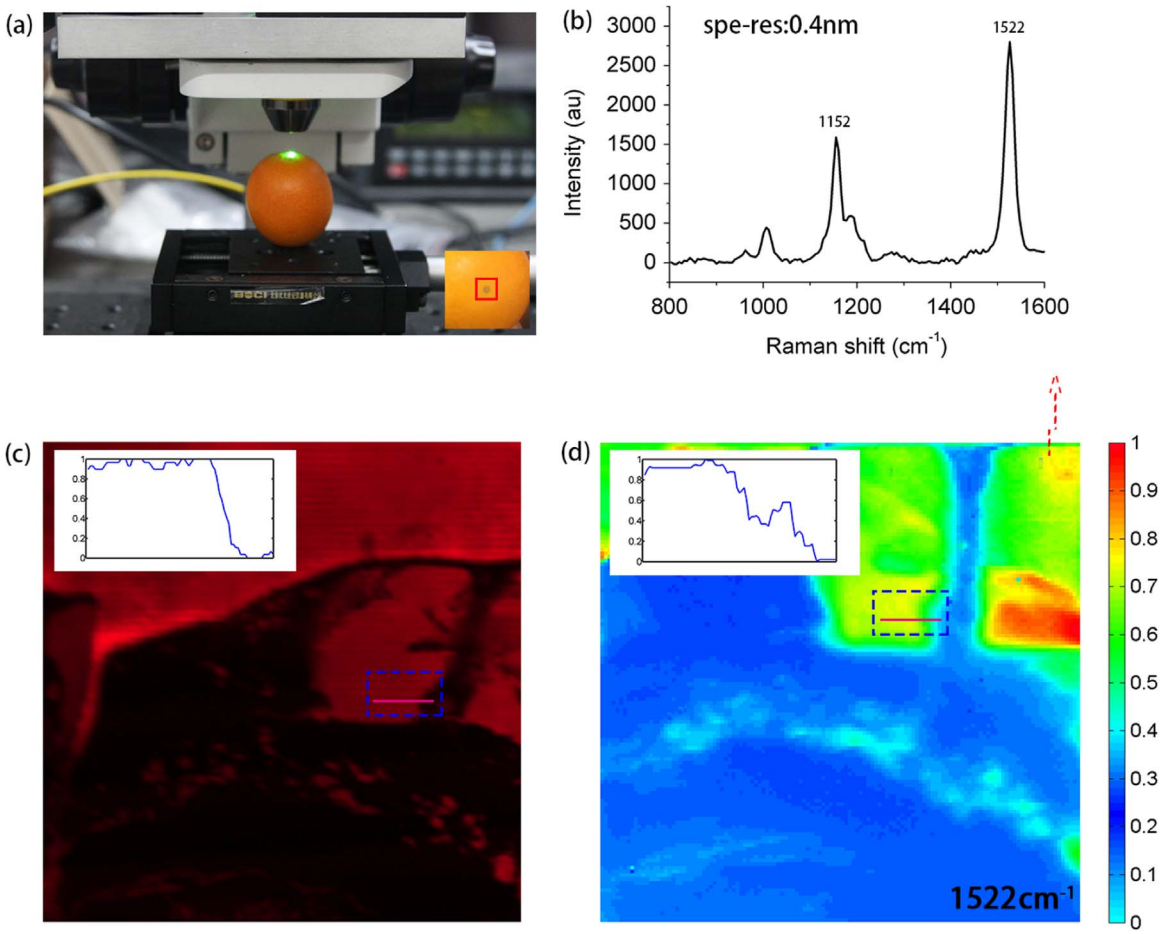

Fig. 6. (a) Schematic of the Raman spectral imaging experiment. Inset: top view of the kumquat, inside the red rectangular region is the scar of the pericarps. (b) Raman spectrum of fresh kumquat. The excitation power in the focal spot is about 50 mW, while spectral resolution (spe-res) is 0.4 nm. The Raman spectrum is baseline corrected [33], with the integral time of 1 s at a single point. (c) Reflectance image of the kumquat. Pixel dwell time: 20 μs, image size: 128×128 pixels. (d) Raman image of the kumquat at 1522 cm^{-1}. Pixel dwell time: 1 s, image size: 128×128 pixels. In the blue dotted rectangular of Fig. 6(c) and (d) are almost the same region of kumquat pericarps. Insets of (c) and (d) show the normalized intensity distributions along the purple line.

intensity, which indicates a different content of carotenoid molecules. This demonstrates that Raman spectral images can provide more abundant information of the sample compared to intensity images. The Raman spectral image of kumquat pericarps suggests that this system has the potential to be used to inspect the distribution of pesticide residues on foods or fruits.

4. Conclusion

The use of in vivo and in situ confocal imaging has spread throughout in many applications, such as life sciences and food safety investigations. In this study, a portable confocal hyperspectral microscope has been developed in laboratory by utilizing cage system components and fiber, without traditional scan and tube lens, to obtain high light detection efficiency. At the same time, the microscope is capable of achieving a lateral resolution superior to 2.19 μm, which is useful in most applications. With a multimode fiber as a pinhole, an improved image contrast is also achieved as shown in Fig. 2.

The relationship between the fluorescence intensity and the optical path are particularly investigated. The logarithm of fluorescence intensity is demonstrated to be linearly negatively correlated to the optical length, addressing the necessity of reducing optical path length.

In this compact microscopy without scan lens and tube lens, the fluorescence intensity has been enhanced, which is significant for the detection of weak signals. In order to demonstrate the effectiveness of this system, the HeLa cell labeled with TTF encapsulated organically modified silica was imaged, which validates the capability of achieving fluorescence images of cells. The confocal in-vivo fluoresce images of fingerprint was also acquired to show the ability of this system in small object imaging. In addition, we experimentally demonstrate the versatility of this system by detecting the weak Raman signal of kumquat pericarps on both intensity imaging and spectral imaging mode. Compared to intensity images, the Raman spectral images can provide more information about molecular in the sample. We believe PCHM has great potential for hyperspectral imaging applications in biological and medical fields, especially combined with plasmonic resonance enhancement technique [31,32]. Besides, the volume of this system can also be further scaled down by employing small customized components. This way, the PCHM can be utilized as site-level equipment in farmland and industrial line. It should be mentioned that due to the large diameter of the pinhole, the depth resolution of the system is decreased, which can be improved by adopting the fiber with smaller core diameter in the further study.

Funding Information

This work is partially supported by “111” Project (B07031; Fundamental Research Funds for the Central Universities), the Program of Zhejiang Leading Team of Science and Technology Innovation (2010R50007), Scientific research fund of Hainan University (kyqd1653) and Changshu Innovative and Entrepreneurship Fund (CSRC1535).

Acknowledgment

The authors would like to thank Wen Liu for discussion in the experiment.

References

[1] N. Uzunbajakava, A. Lenferink, Y. Kraan, E. Volokhina, G. Vrensen, J. Greve, C. Otto, Nonresonant confocal Raman imaging of DNA and protein distribution in apoptotic cells, Biophys. J. 84 (2003) 3968–3981.
[2] S. Keren, C. Zavaleta, Z. Cheng, A. de La Zerda, O. Gheysens, S. Gambhir, Noninvasive molecular imaging of small living subjects using Raman spectroscopy, Proc. Natl. Acad. Sci. 105 (2008) 5844–5849.
[3] S. Deng, L. Liu, Z. Liu, Z. Shen, G. Li, Y. He, Line-scanning Raman imaging spectroscopy for detection of fingerprints, Appl. Opt. 51 (2012) 3701–3706.
[4] J. Ling, S.D. Weitman, M.A. Miller, R.V. Moore, A.C. Bovik, Direct Raman imaging techniques for study of the subcellular distribution of a drug, Appl. Opt. 41 (2002) 6006–6017.
[5] S.F. El-Mashtoly, H.K. Yosef, D. Petersen, L. Mavarani, A. Maghnouj, S. Hahn, C. Kötting, K. Gerwert, Label-free Raman spectroscopic imaging monitors the integral physiologically relevant drug responses in cancer cells, Anal. Chem. 87 (2015) 7297–7304.
[6] E. Karavas, M. Georgarakis, A. Docoslis, D. Bikiaris, Combining SEM, TEM, and micro-Raman techniques to differentiate between the amorphous molecular level dispersions and nanodispersions of a poorly water-soluble drug within a polymer matrix, Int. J. Pharm. 340 (2007) 76–83.
[7] E. Widjaja, W.L. Lee, S.C.J. Loo, Application of Raman microscopy to biodegradable double-walled microspheres, Anal. Chem. 82 (2009) 1277–1282.
[8] K.B. Biggs, K.M. Balss, C.A. Maryanoff, Pore networks and polymer rearrangement on a drug-eluting stent as revealed by correlated confocal Raman and atomic force microscopy, Langmuir 28 (2012) 8238–8243.
[9] J. Qin, K. Chao, M. Kim, Raman chemical imaging system for food safety and quality inspection, Trans. ASABE 53 (2010) 1873–1882.
[10] J. Qin, K. Chao, M.S. Kim, Investigation of Raman chemical imaging for detection of lycopene changes in tomatoes during postharvest ripening, J. Food Eng. 107 (2011) 277–288.
[11] T.C. Rich, N. Annamdevula, A.L. Britain, S. Mayes, P.F. Favreau, S.J. Leavesley, Three dimensional measurement of cAMP gradients using hyperspectral confocal microscopy, in: SPIE BiOS, International Society for Optics and Photonics, 2016, pp. 97130O-97130O-97135.
[12] J. Qin, K. Chao, M.S. Kim, A line-scan hyperspectral system for high-throughput Raman chemical imaging, Appl. Spectrosc. 68 (2014) 692–695.
[13] J. Qin, K. Chao, M.S. Kim, B.-K. Cho, Line-Scan Macro-scale Raman chemical imaging for authentication of powdered foods and ingredients, Food Bioprocess Technol. 9 (2016) 113–123.
[14] J. Qi, W.-C. Shih, Performance of line-scan Raman microscopy for high-throughput chemical imaging of cell population, Appl. Opt. 53 (2014) 2881–2885.
[15] S.D. Schwab, R.L. McCreery, Versatile, efficient Raman sampling with fiber optics, Anal. Chem. 56 (1984) 2199–2204.
[16] M.G. Shim, B.C. Wilson, E. Marple, M. Wach, Study of fiber-optic probes for in vivo medical Raman spectroscopy, Appl. Spectrosc. 53 (1999) 619–627.
[17] H.P. Buschman, E.T. Marple, M.L. Wach, B. Bennett, T.C. Bakker Schut, H.A. Bruining, A.V. Bruschke, A. van der Laarse, G.J. Puppels, In vivo determination of the molecular composition of artery wall by intravascular Raman spectroscopy, Anal. Chem. 72 (2000) 3771–3775.
[18] J.T. Motz, M. Hunter, L.H. Galindo, J.A. Gardecki, J.R. Kramer, R.R. Dasari, M.S. Feld, Optical fiber probe for biomedical Raman spectroscopy, Appl. Opt. 43 (2004) 542–554.
[19] Y. Komachi, H. Sato, K. Aizawa, H. Tashiro, Micro-optical fiber probe for use in an intravascular Raman endoscope, Appl. Opt. 44 (2005) 4722–4732.
[20] M.A. Short, S. Lam, A. McWilliams, J. Zhao, H. Lui, H. Zeng, Development and preliminary results of an endoscopic Raman probe for potential in vivo diagnosis of lung cancers, Opt. Lett. 33 (2008) 711–713.
[21] Y. Komachi, T. Katagiri, H. Sato, H. Tashiro, Improvement and analysis of a micro Raman probe, Appl. Opt. 48 (2009) 1683–1696.
[22] A. Mahadevan-Jansen, M.F. Mitchell, N. Ramanujam, U. Utzinger, R. Richards-Kortum, Development of a fiber optic probe to measure NIR Raman spectra of cervical tissue in vivo, Photochem. Photobiol. 68 (1998) 427–431.
[23] S. Christesen, B. Maciver, L. Procell, D. Sorrick, M. Carrabba, J. Bello, Nonintrusive analysis of chemical agent identification sets using a portable fiber-optic Raman spectrometer, Appl. Spectrosc. 53 (1999) 850–855.
[24] Z. Huang, H. Zeng, I. Hamzavi, D.I. McLean, H. Lui, Rapid near-infrared Raman spectroscopy system for real-time in vivo skin measurements, Opt. Lett. 26 (2001) 1782–1784.
[25] Z. Zhu, X. Zhao, W. Qin, G. Chen, J. Qian, Z. Xu, Fluorescent AIE dots encapsulated organically modified silica (ORMOSIL) nanoparticles for two-photon cellular imaging, Sci. China Chem. 56 (2013) 1247–1252.
[26] C.-K. Hsu, S.-Y. Tzeng, C.-C. Yang, J.Y.-Y. Lee, L.L.-H. Huang, W.-R. Chen, M. Hughes, Y.-W. Chen, Y.-K. Liao, S.-H. Tseng, Non-invasive evaluation of therapeutic response in keloid scar using diffuse reflectance spectroscopy, Biomed. Opt. Express 6 (2015) 390.
[27] S.Y. Tzeng, J.Y. Guo, C.C. Yang, C.K. Hsu, H.J. Huang, S.J. Chou, C.H. Hwang, S.H. Tseng, Portable handheld diffuse reflectance spectroscopy system for clinical evaluation of skin: a pilot study in psoriasis patients, Biomed. Opt. Express 7 (2016) 616–628.
[28] Y.-F. Hsieh, M. Ou-Yang, J.-R. Duann, J.-C. Chiou, N.-W. Chang, C.-I. Jan, M.-H. Tsai, S.-D. Wu, Y.-J. Lin, C.-C. Lee, Development of a novel embedded relay lens microscopic hyperspectral imaging system for cancer diagnosis: use of the mice with oral cancer to be the example, Int. J. Spectrosc. 2012 (2012).
[29] ER. Menzel, Detection of latent fingerprints by laser-excited luminescence, Anal. Chem. 61 (1989) 557A–561A.
[30] F. Schulte, J. Mäder, L.W. Kroh, U. Panne, J. Kneipp, Characterization of pollen carotenoids with in situ and high-performance thin-layer chromatography supported resonant Raman spectroscopy, Anal. Chem. 81 (2009) 8426–8433.
[31] J. Lin, Y. Zhang, E.-H. Lee, S. He, A triple-resonance Raman chip for simultaneous enhancement of Stokes and anti-Stokes lines utilizing both localized and non-localized plasmonic resonance, J. Opt. 17 (2015) 105001.
[32] Z. Yong, S. Zhang, Y. Dong, S. He, Broadband nanoantennas for plasmon enhanced fluorescence and raman spectroscopies, Prog. Electromagn. Res. 153 (2015) 123–131.
[33] F. Gan, G. Ruan, J. Mo, Baseline correction by improved iterative polynomial fitting with automatic threshold, Chemom. Intell. Lab. Syst. 82 (2006) 59–65.